International Journal of Remote Sensing
Vol. 30, No. 9, 10 May 2009, 2337–2354

Radiometric surface temperature calibration effects on satellite based evapotranspiration estimation

J. L. CHÁVEZ*, P. H. GOWDA, T. A. HOWELL and K. S. COPELAND
Conservation and Production Research Laboratory, USDA-ARS, PO Drawer 10, Bushland, TX 79012, USA

(*Received 12 October 2007; in final form 21 June 2008*)

Agriculture on the Texas High Plains (THP) uses approximately 89% of groundwater withdrawals from the Ogallala Aquifer, leading to steady decline in water table levels. Therefore, efficient water management is essential for sustaining agricultural production in the THP. Accurate evapotranspiration (ET) maps provide critical information on actual spatio-temporal crop water use. METRIC (Mapping Evapotranspiration at High Resolution using Internalized Calibration) is a remote sensing based energy balance method that uses radiometric surface temperature (T_s) for mapping ET. However, T_s calibration effects on satellite based ET estimation are less known. Further, METRIC has never been applied for the advective conditions of the semi-arid THP. In this study, METRIC was applied and predicted ET was compared with measured values from five monolithic weighing lysimeters at the USDA-ARS Conservation and Production Research Laboratory in Bushland, Texas, USA. Three different levels of calibration were applied on a Landsat 5 Thematic Mapper's thermal image acquired on 23 July 2006 to derive T_s. Application of METRIC on a MODTRAN calibrated image improved the accuracy of distributed ET prediction. In addition, ET estimates were further improved when a THP-specific model was used for estimating leaf area index. Results indicated that METRIC performed well with ET mean bias error $\pm$ root mean square error of $0.4 \pm 0.7\,\mathrm{mm\,d^{-1}}$.

1. Introduction

The Ogallala Aquifer is the main source of water supply for the Texas High Plains (THP) and it is being depleted at an unsustainable rate (Axtell 2006). In the THP, irrigation alone uses approximately 89% of the water pumped from the Ogallala Aquifer (Dennehy 2000). McGuire (2004) indicated that the change in water storage in the aquifer beneath the THP, from predevelopment to 2003, was about 164.1 $\mathrm{km^3}$ (5.2 $\mathrm{km^3}$ from 2002 to 2003) with an average area-weighted water-level decline of 10.6 m (0.37 m from 2002 to 2003). For this reason and considering the positive trends in population growth in the THP, there is a need for greater efficiency in irrigation water management for agriculture.

Improvement in irrigation water management may be achieved when the beneficial crop water use, among other factors, is accurately quantified in time and space. Remote sensing (RS) based evapotranspiration (ET) methods are found to be useful for deriving such information. Numerous RS algorithms, such as METRIC (Mapping Evapotranspiration at high Resolution with Internal

*Corresponding author. Email: jose.chavez@ars.usda.gov

International Journal of Remote Sensing
ISSN 0143-1161 print/ISSN 1366-5901 online © 2009 Taylor & Francis
http://www.tandf.co.uk/journals
DOI: 10.1080/01431160802549393

Calibration; Trezza 2002, Allen *et al.* 2007a, 2005a), SEBAL (Surface Energy Balance for Land; Bastiaanssen *et al.* 1998), a two-source energy balance model (TSM; Norman *et al.* 1995), a dimensionless temperature method (Δ_T, Suleiman and Crago 2004), an aerodynamic temperature-based model (Chávez 2005, Chávez *et al.* 2005) and an analytical land atmosphere radiometer model (ALARM; Suleiman and Crago 2002) have been developed to spatially estimate crop water consumption or ET and are being tested around the world. These algorithms mainly solve the energy balance of the land surface for latent heat flux (LE), equation (1), at the time of satellite or airborne RS system overpass and extrapolate instantaneous LE to daily ET values.

$$\mathrm{LE} = R_n - G - H, \tag{1}$$

where R_n is net radiation ($\mathrm{W\,m^{-2}}$), G is the soil heat flux ($\mathrm{W\,m^{-2}}$) and H is the sensible heat flux ($\mathrm{W\,m^{-2}}$). LE is converted to ET ($\mathrm{mm\,h^{-1}}$ or $\mathrm{mm\,d^{-1}}$) by dividing it by the latent heat of vaporization (λ_{LE}=2.501–0.00236 (T_a), $\mathrm{MJ\,kg^{-1}}$ for T_a in °C), density of water (ρ_w; ~1.0 $\mathrm{Mg\,m^{-3}}$), and an appropriate time constant. The sign convention for the different flux terms in equation (1) is positive from the land surface to the atmosphere (up) for LE and H, and positive towards the surface for R_n and into the ground (down) for G.

Gowda *et al.* (2007a) discussed the pros and cons of numerous RS algorithms for ET estimation. For instance, they indicated that the TSM model yielded surface heat fluxes with errors within 10–12%, although this model demands several crop and micro-meteorological data that, in many circumstances, are very difficult to obtain. The SEBAL model had a typical accuracy of 85% or errors ranging from 2.7 to 35.0% with an overall average error of 18.2%, under a variety of climatic/environmental conditions. METRIC appeared to have an advantage over SEBAL under advective conditions. METRIC's ET estimation errors were reported to be approximately 10–20% for daily estimates and as low as 1–4% for seasonal ET estimates, requiring only vapour pressure (or relative humidity) and wind speed measurements from weather stations (WS) within the satellite scene. Therefore, the attributes presented by METRIC make it very attractive for mapping ET under the advective conditions regularly encountered in the THP.

Allen *et al.* (2005b) stated that 'The result of no correction of L_6 (radiance values in thermal band 6 of Landsat Thematic Mapper) will be a general underestimation of surface temperature (T_s) by up to about 5°C for warmer portions of an image. However, because METRIC tailors the "dT" function around the T_s data calculated for an image, the impact on final ET values is generally small, especially for areas having low and high values of ET. Errors may be larger for midrange ET values, but generally less than a few percent'. Tasumi *et al.* (2005) performed a sensitivity analysis and concluded that the internal calibration procedures in METRIC largely eliminate errors in ET resulting from lack of atmospheric corrections. However, inaccurate calibrated T_s values for the hot and cold pixels may scale dT (Allen *et al.* 2005b) inappropriately. Thus, error accumulation in R_n, G and H may affect ET estimation accuracy through error propagation. Therefore, it is of interest to evaluate the effect of using different levels of T_s calibration. It involves the removal of atmospheric effects on the at-sensor apparent temperature. Atmospheric effects include atmospheric (gases) interception of some thermal radiation emitted by the surface and some thermal radiation emission by the atmosphere towards the remote sensor and towards the land surface.

Leaf area index (LAI) is a measure of foliage density that plays a major role in photosynthesis, groundwater-surface water interactions through ET (Summer and

Jacobs 2005). In addition, the roughness length for momentum transfer (Z_{om}) also affects ET because it influences the surface turbulence, which is the key mechanism of momentum exchange between the atmosphere and land surface (Yang and Friedl 2002). Borak *et al.* (2005) stated that Z_{om} is the height above the surface at which the mean logarithmic wind profile theoretically reaches zero. Both LAI and Z_{om} remote sensing-based models may be region-specific since soil background effects may affect these models' performance. Therefore, incorporation of locally developed LAI and Z_{om} models in METRIC is desirable to assess the ability of the 'dT' mechanism to accurately estimate daily ET.

The THP is a semi-arid region with heterogeneous landscapes in which irrigated fields are surrounded by dryland crops, fallow land, and/or rangeland. Therefore, the advection of hot air from dry surfaces is a significant source of energy that has a major impact on ET from crop growing areas. For example, Tolk *et al.* (2006) reported an average ET rate of 11.3 mm d^{-1}, measured with a large weighing lysimeter, for irrigated alfalfa in Bushland, Texas, with ET for some days exceeding 15 mm d^{-1} due to regional advection. The main objective of this study was to assess the effects of different levels of radiometric surface temperature calibration on METRIC ET estimation accuracy in the THP. We selected METRIC for its ability to yield accurate ET estimations under advective conditions with minimal ground-based weather data. In addition, the effect on estimated ET of locally developed LAI and Z_{om} models was also studied.

2. Materials and methods

2.1 *Study area*

This study was conducted at the Conservation and Production Research Laboratory (CPRL), USDA-ARS located in Bushland, Texas, USA (figure 1). The geographic coordinates of the CPRL are 35°11′ N, 102°06′ W, and its elevation is 1170 m above mean sea level. For this study, a 30-m resolution Landsat 5 TM scene was used to derive energy fluxes at the land surface. The scene path/row was 31/36 and was acquired at 17:20 GMT (11:20 am Central Standard Time (CST) in the US) on 23 July 2006 (DOY 204). The TM band 6 image was captured at a coarser resolution of 120 m, and was re-sampled to 30 m by the image supplier. Soils around Bushland are classified as slowly permeable Pullman clay loam soils. The major crops in the THP are corn, sorghum, winter wheat and cotton. Weather conditions during the Landsat 5 overpass, at the Bushland-ARS grass reference ET weather station, which is a part of the Texas High Plains ET Network (TXHPET 2006), included clear sky with incoming short wave radiation of 907 W m^{-2}, air temperature of 29°C, low relative humidity of 32%, wind speed of 3 m s^{-1}, and soil temperatures of 29°C and 28°C at 5 cm and 15 cm depth, respectively.

METRIC estimated ET values were verified by comparing them with soil water mass change-based daily ET values from five monolithic precision weighing lysimeters located at the CPRL (figure 2). Four large lysimeters (3 m length × 3 m width × 2.5 m depth) were each located in the middle of 4.7-ha fields. In 2006, two fields (SW and NW) were planted to dryland grain sorghum with the NW field planted in clumps as part of another study. The irrigated SE and NE lysimeter fields were planted to forage sorghum and corn, respectively. One lysimeter was 1.5 m by 1.5 m by 2.5 m deep and was located in the grass reference ET weather station field (0.31 ha), (TXHPET 2006). Each of the four lysimeter fields was equipped with one

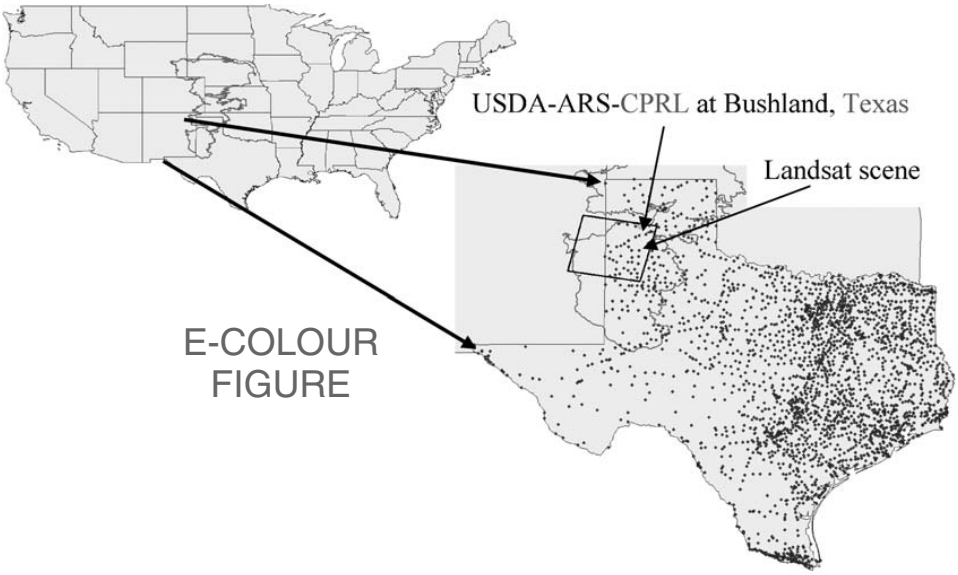

Figure 1. Landsat 5 TM path/row 31/36 scene (rectangle) covering an area underlaid by the Ogallala Aquifer (irregular polygon) in the Texas High Plains (Panhandle). The USDA-ARS-CPRL laboratory location is indicated by a dot.

net radiometer (Q*7.1, Radiation and Energy Balance Systems (REBS)[†] Seattle, Washington) and one infrared thermometer (IRT) (2G-T-80F/27C, Exergen, Watertown, Massachusetts) for measuring net radiation and surface temperature, respectively. On the grass lysimeter, only net radiation was measured.

2.2 *Lysimeter set-up*

Each of the four large lysimeters at Bushland contains a monolithic Pullman clay loam soil core. Change in the soil water mass was used for determining ET values. Changes in lysimeter mass were determined using a data logger (model CR7-X, Campbell Scientific, Inc., Logan, Utah) to measure and record the lysimeter load cell (model SM-50, Interface, Scottsdale, AZ) with the signal sampled at a frequency of 0.17 Hz (every 6 s). The lysimeters were calibrated using techniques similar to those found in Howell *et al.* (1995). The lysimeter mass measurement accuracy in water depth equivalent was 0.01 mm, as indicated by the root mean squared error of calibration. The load cell signal was averaged for 5 min and composited to 60-min means. The lysimeter mass data were reported on the midpoint of the 60 min, that is, data were averaged from 0 to 60 min and reported at the midpoint of the averaging period. Daily ET was calculated as the difference between lysimeter mass recorded at 2330 h CST of one day and 2330 h CST of the next day to determine mass losses (from evaporation and transpiration) to which lysimeter mass gains (from irrigation or precipitation) were added. A vacuum pump regulated to -10 kPa provided drainage, and the drainage effluent was held in two tanks suspended from each lysimeter and weighed with load cells.

[†]Mention of trade or commercial products in this article is solely for the purpose of providing specific information and does not imply recommendation or endorsement by the US Department of Agriculture.

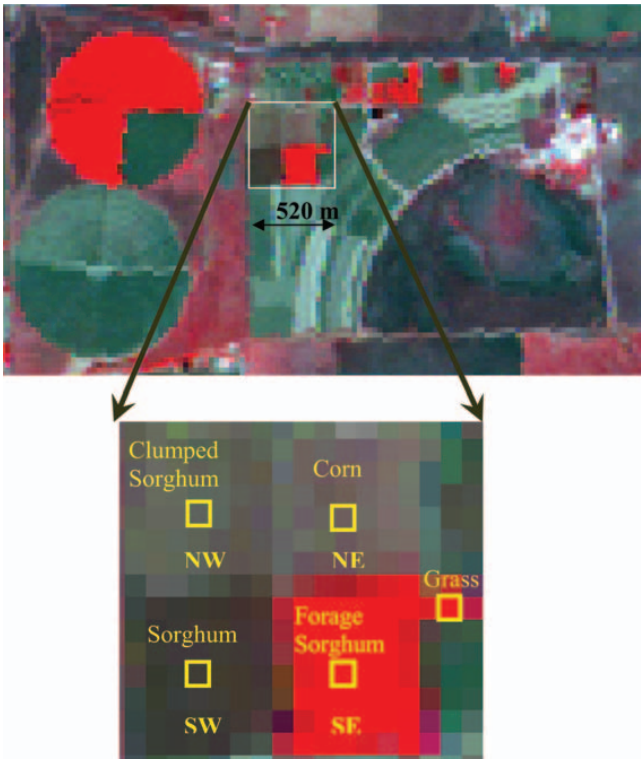

COLOUR FIGURE

Figure 2. Landsat 5 TM false colour image showing lysimeter locations at USDA-ARS-CPRL facility in Bushland, TX.

2.3 *Satellite image radiometric and atmospheric calibration*

METRIC requires radiometric and atmospheric calibration of satellite images for estimating spatial ET. Detailed steps on the Landsat 5 TM radiometric calibration procedures can be found in Chander and Markham (2003). In short, the digital numbers (DN) stored in the satellite image were first converted into radiance (L_b), for each band as $L_b = (\text{gain} \times \text{DN}) + \text{bias}$). Then at-sensor or top-of-atmosphere (TOA; exo-atmospheric) reflectance values for the shortwave bands were estimated. Reflectance values were calculated by dividing the detected radiance at the satellite (for each band) by the incoming energy (radiance) in the same shortwave band. The incoming radiance is a function of mean solar exo-atmospheric irradiance, solar incidence angle, and the inverse square of the relative earth-to-sun distance. In the case of the thermal band, the spectral radiance values were converted into effective at-satellite temperatures of the viewed earth-atmosphere system under an assumption of unity for surface emissivity and using pre-launch calibration constants by means of an inverted logarithmic formula. Subsequently, surface reflectance values were computed after applying atmospheric interference corrections, on the TOA reflectance image, for shortwave absorption and scattering using narrowband transmittance values for each band as calibrated by Tasumi *et al.* (2005). They used radiative transfer models such as SMARTS2 (Gueymard 1995) and MODTRAN3 (Berk *et al.* 1989) in their calibration. Surface temperature was obtained after correcting the at-satellite effective 'brightness' temperatures for surface emissivity only.

2.4 *METRIC algorithm*

In METRIC, ET is computed as a residual from the surface energy balance equation as an instantaneous ET or latent heat flux (LE) as shown in equation (1). R_n is calculated using surface reflectance and radiometric surface temperature (T_s) derived from satellite imagery, near-surface vapour pressure from a nearby weather station (WS), and R_s as explained below. R_n is the result of the surface energy budget between short and long wave radiation terms, described as:

$$R_n = R_s\downarrow - \alpha R_s\downarrow + R_L\downarrow - R_L\uparrow - (1-\varepsilon_o)R_L\downarrow \tag{2}$$

where $R_s\downarrow$ is incoming shortwave radiation ($\mathrm{W\,m^{-2}}$). In this study $R_s\downarrow$ was not estimated as indicated in Allen *et al.* (2005a, 2007a) but rather measured with a pyranometer (model CMP 6, Kipp and Zonen, Bohemia, NY) installed at the USDA-ARS-CPRL weather station (TXHPET 2006). Surface albedo, α, is a function of surface reflectance values in the shortwave portion of the electromagnetic spectrum (a weighted average of reflectance in TM bands 1, 2, 3, 4, 5 and 7), and dimensionless; it is estimated following the procedure of Allen *et al.* (2007a). $R_L\downarrow$ is incoming long wave radiation ($\mathrm{W\,m^{-2}}$) or downward thermal radiation flux originated from the atmosphere, which was estimated using the Stefan-Boltzmann equation and near surface air temperature as well as vapour pressure for sky emissivity. In METRIC, $R_L\downarrow$ is estimated using T_s and atmospheric (sky) thermal emissivity (which is a function of atmospheric transmissivity for shortwave radiation). $R_L\uparrow$ is outgoing long wave radiation ($\mathrm{W\,m^{-2}}$), a function of T_s and broadband surface thermal emissivity (ε_o, dimensionless). The ε_o term is a function of biomass or LAI presence and was calculated using empirical equations developed by Tasumi *et al.* (2005) based on soil and vegetation thermal spectral emissivities. The $(1-\varepsilon_o)R_L\downarrow$ term represents the fraction of incoming long wave radiation reflected from the surface.

Soil heat flux was modelled as a function of R_n, vegetation index, T_s, and α for near midday values (Bastiaanssen 2000):

$$G = \left((T_s - 273.15)(0.0038 + 0.0074\,\alpha)\left(1 - 0.98\ \mathrm{NDVI}^4\right)\right)R_n, \tag{3}$$

where NDVI is the Normalized Difference Vegetation Index [(R-NIR)/(R + NIR)], R is reflectance in the red band and NIR is reflectance in the near infrared band.

Sensible heat flux is defined by the bulk aerodynamic resistance equation, which uses aerodynamic temperature (T_{aero}) and aerodynamic resistance to heat transfer (r_{ah}):

$$H = \rho_a\, Cp_a (T_{aero} - T_a)/r_{ah}, \tag{4}$$

where ρ_a is air density ($\mathrm{kg\,m^{-3}}$), Cp_a is specific heat of dry air ($1004\,\mathrm{J\,kg^{-1}\,K^{-1}}$), T_a is average air temperature (K), T_{aero} is average aerodynamic temperature (K), which is defined for a uniform surface as the temperature at the height of the zero plane displacement (d, m) plus the roughness length (Z_{oh}, m) for sensible heat transfer, and r_{ah} is aerodynamic resistance ($\mathrm{s\,m^{-1}}$) to heat transfer from Z_{oh} to Z_m (height of wind speed measurement, in m).

In METRIC, H is estimated without needing to know T_a or T_{aero}; instead a temperature difference ($\mathrm{d}T$), a function of T_s, is used, as:

$$H = \rho_a Cp_a \frac{\mathrm{d}T}{r_{ah}} \tag{5}$$

where r_{ah} is calculated between two near surface heights, z_1 and z_2 (generally 0.1 and 2.0 m) using a wind speed extrapolated from some blending height above the ground surface (typically 100 to 200 m) and an iterative stability correction scheme for atmospheric heat transfer based on the Monin-Obhukov stability length scale (L_{MO}, similarity theory; Foken 2006). In this study, a height of 200 m was used in the calculation of distributed friction velocity (u_*), a term utilized in the estimation of H.

Allen *et al.* (2007a) explained that dT (K) represents the near-surface temperature difference between z_1 and z_2, and that the indexing of dT to T_s does not rely on absolute values of T_s, which allegedly reduces the error in calculating H substantially. Equation (6) characterizes the relationship of dT to T_s (Bastiaanssen 1995).

$$dT = a + b\ T_s, \tag{6}$$

where a and b are empirically determined constants. The determination of a and b in equation (6) involves locating a hot (dry) pixel in a fallow agricultural field with large T_s and a cold (wet) pixel with a small T_s (typically one in an irrigated agricultural setting) in the remote sensing image. Once these pixels have been identified, the energy balance of equation (1) can be solved for H_{cold} and H_{hot} as:

$$H_{cold} = (R_n - G)_{cold} - LE_{cold} \tag{7}$$

$$H_{hot} = (R_n - G)_{hot} - LE_{hot}, \tag{8}$$

where H_{hot} and H_{cold} are the sensible heat fluxes for the hot and cold pixels, respectively. The hot pixel is defined as having $LE_{hot}=0$, which means that all available energy is partitioned to H. However, LE_{hot} may be non-zero and calculated according to a soil water budget if significant rainfall has occurred shortly before the image acquisition date. The cold pixel is assumed to have an LE value equal to 1.05 times that expected for a tall reference crop (i.e. alfalfa), thus LE_{cold} is set equal to 1.05 $ET_r\ \lambda_{LE}$, where ET_r is the hourly (or shorter time interval) tall reference (like alfalfa) ET calculated using the standardized ASCE Penman-Monteith equation (ASCE-EWRI 2005). A 1.05 coefficient was used to estimate LE_{cold} as the cold pixels typically have an ET rate of 5% larger than that for the reference ET (ET_r) due to wet soil surface beneath a full vegetation canopy that will tend to increase the total ET rate (Allen *et al.* 2007a).

The hot pixel was chosen after careful screening of fallow/bare agricultural fields displaying high temperatures, high albedo and low biomass (low LAI); these values are shown in Table A1 (Appendix A). With the calculation of H_{hot} and H_{cold}, equation (5) was inverted to compute dT_{hot} and dT_{cold}. The a and b coefficients were then determined by fitting a line through the two pairs of values for dT and T_s from the hot and cold pixels. These a and b values were initial estimates that were used in an iterative stability correction scheme programmed in a Microsoft Excel™ spreadsheet, which after some iterations shows numerical convergence. The a and b coefficients for each iteration were then exported to a model in Leica ERDAS Imagine to obtain the final stability corrected H image.

Instantaneous LE image values were obtained using equation (1) and were converted to ET_i in mm h^{-1} by division by λ_{LE} and ρ_w. In METRIC, λ_{LE} is calculated substituting T_a by T_s

$$ET_i = 3600\ LE / \{[2.501 - 0.00236(T_s - 273.15)](10^6)(1.0)\} \tag{9}$$

Reference ET fraction (ET_rF) is the ratio of ET_i to the reference ET_r that is computed from weather station data at overpass time (hourly average). The weather

station information is explained in a subsequent section. Finally, the computation of daily or 24-h ET (ET_d), for each pixel, is performed as:

$$ET_d = ET_r F \times ET_r 24 \tag{10}$$

where: ET_r24 is the cumulative 24-h ET_r for the day (mm d^{-1}).

2.5 *Reference ET weather station data*

For the calculation of ET_r and ET_r24 for alfalfa, weather data recorded by the USDA-ARS (Bushland) reference WS located on a grass field was used (TXHPET 2006). The TXHPET reported hourly and daily weather data for the calculation of the grass (ET_o) and alfalfa (ET_r) reference ET by means of the standardized ASCE Penman-Monteith method (ASCE-EWRI 2005). ET_r was 9.2 mm d^{-1} and ET_o was 7.3 mm d^{-1} on DOY 204.

2.6 *METRIC ET estimation evaluation*

Considering the large range of surface temperatures and the potential impact that atmospheric effects could have in determining accurate radiometric surface temperature in semi-arid regions, a comparison between T_s calibrated using the METRIC method and measured values using ground-based IRTs (surface emissivity corrected) was performed. Also, at-sensor (at-satellite or TOA) surface brightness temperatures were corrected for atmospheric effects and surface emissivity using MODTRAN4 Version3 (Berk *et al.* 2003), including weather station-based atmospheric profile, and results were compared with the same ground-based IRT readings.

For application of METRIC, radiometric surface temperature was estimated using three different techniques: (a) corrected with a submodel provided in the METRIC procedure that corrects at-sensor surface brightness temperatures for narrow-band surface thermal emissivity only (named T_s(ME)); (b) at-sensor surface brightness temperature values without any surface emissivity or atmospheric effects correction (named T_B); and (c) radiometric surface temperature corrected for atmospheric and surface thermal emissivity effects with MODTRAN4 (named T_s(MO)). In addition, T_s(MO) plus a THP-specific LAI model (Gowda *et al.* 2007b) and a locally adjusted surface roughness for momentum transfer model (named T_s(MO2)) was used in the estimation of ET. The THP-specific LAI model used in this study was:

$$\mathrm{LAI} = 8.768 \times (\mathrm{NDVI})^{3.616}. \tag{11}$$

The surface roughness length for momentum transfer used in method T_s(MO2) was obtained by calibrating the linear equation $Z_{om}=a+b$ LAI using Brutsaert's (1982) predicted Z_{om} values ($Z_{om}=0.123\ h_c$), measured crop height (h_c, m) and LAI values (from the SE forage sorghum field). The intercept, a, for the linear Z_{om} equation, was constrained to a value of 0.004 m, as a minimum value for a bare soil or fallow field in an agricultural setting.

$$Z_{om} = 0.004 + 0.035\ \mathrm{LAI} \tag{12}$$

Comparisons of predicted T_s, R_n, and ET_d with measured values were made. Estimates of LAI using the METRIC model (LAI(ME), equation (13)) and LAI obtained using equation (11), called LAI(THP), were compared in order to appreciate the differences in these models. For the verification of METRIC

estimated surface albedo, estimates were compared to reference values derived from the Kipp and Zonen net radiometers installed in lysimeter fields by dividing incoming shortwave radiation by reflected radiation at satellite overpass time (11:20 am CST).

The LAI submodel provided in the METRIC algorithm is:

$$\mathrm{LAI(ME)} = -\ln[(0.69 - \mathrm{SAVI_{ID}})/0.59]/0.91, \tag{13}$$

where $\mathrm{SAVI_{ID}}$ is the Soil Adjusted Vegetation Index for southern Idaho [SAVI=(1+0.1) (R−NIR)/(0.1+R+NIR)].

Results of the comparison of ET using METRIC and ET at each lysimeter location (one pixel value, as shown in figure 2) were reported as absolute differences and in per cent errors:

$$\text{Per cent error}(\%) = (\mathrm{ET_ME} - \mathrm{ET_L}) \times 100/\mathrm{ET_L}, \tag{14}$$

where ET(ME) is the ET estimated by METRIC and ET(L) is ET derived from the lysimeter's water mass loss/gain data. A more comprehensive evaluation of ET estimation errors (comparison of estimated/measured ET) was carried out comparing mean bias error (MBE) and root mean square error (RMSE).

3. Results and discussion

3.1 *Surface temperature*

MODTRAN generated T_s(MO) values within the Landsat 5 TM scene ranged from 17.9°C at Ute Lake (north-eastern New Mexico, about 165 km west of Bushland, Texas) to 46.4°C over bare soils, a difference of 28.5°C. T_s(MO) values compared better with measured data than did T_s(ME) values. Errors of T_s(MO) values were −0.7°C (−1.9%) and −0.2°C (0.4%) for NE and SE lysimeter fields, respectively, while errors of the METRIC submodel (T_s(ME)) were −3.9°C (−11.1%) and (−1.9%) for the same fields (table 1). A larger error was found with T_s(ME) on the low biomass NE lysimeter field planted to corn. The low biomass on NE lysimeters was due to late planting of corn (3 July). Corn had been initially planted on 11 May but it suffered severe damage due to heavy hail and had to be re-planted. The larger error for T_s(ME) may be because the T_s correction submodel in METRIC includes only surface thermal emissivity correction, neglecting atmospheric interference effects. In the case of T_B, the temperature difference on the NE lysimeters was −20.8% and −8.0% on the SE lysimeter. T_s(MO2) values were not significantly different than those of T_s(MO). Table 1 does not include data from the grass, NW and SW lysimeter fields because IRT data were not available for DOY 204 on those fields. The grass lysimeter did not have an IRT sensor.

3.2 *Net radiation estimation*

Remote sensing based R_n estimates (table 2), using inputs from the four different methods (a, b, c, and d) resulted in larger bias for the uncalibrated T_B method. Its corresponding error was $59.0 \pm 17.7\,\mathrm{W\,m^{-2}}$ and only $25.3 \pm 19.4\,\mathrm{W\,m^{-2}}$ for T_s(MO2) (average per cent errors are given in table 2). These results signify an improvement in R_n estimates over the T_B method results, of $0.5 \pm 0.1\%$ for T_s(ME), $1.1 \pm 0.4\%$ for T_s(MO), and $5.9 \pm 0.2\%$ for T_s(MO2) respectively. The MBE for method T_s(MO2) was 50% lower than that with T_s(ME) indicating that with

Table 1. Comparison of T_s(ME), T_B, T_s(MO), and T_s(MO2) values with ground-based IRT measurements (T_s(IRT)), at the time of satellite overpass[a].

	T_s (°C)		Diff[b] (°C)		Diff (%)	
	NE	SE	NE	SE	NE	SE
T_s(IRT)	34.8	27.1	0.0	0.0	0.0	0.0
T_B	28.8	25.1	−6.0	−2.0	−20.8	−8.0
T_s(ME)	30.9	26.5	−3.9	−0.6	−12.6	−2.3
T_s(MO)	34.1	27.3	−0.7	0.2	−2.1	0.7
T_s(MO2)	33.8	27.3	−1.0	0.2	−3.0	0.7

[a] T_s(IRT) is ground-level infrared thermometer surface temperature (measured), T_B is at-sensor surface brightness temperature, T_s(ME) is METRIC-based surface temperature; T_s(MO) is MODTRAN-based surface temperature; and T_s(MO2) is MODTRAN-based surface temperature utilizing local LAI and Z_{om} models.
[b] Diff=difference between observed and measured values.

MODTRAN calibrated T_s and a region-specific LAI models may be needed for improving accuracy of spatially distributed R_n estimates. R_n estimation errors progressively decreased with greater T_s calibration (table 2). However, these improvements on R_n estimates were not statistically significant.

Overestimation of R_n by R_n(ME) compared with R_n(MO2) was probably due to errors introduced in the computation of $R_{lw}\downarrow$ and $R_{lw}\uparrow$. In $R_{lw}\downarrow$ calculation, METRIC replaces T_a by T_s and estimates atmospheric (air) emissivity (ε_a) based on an estimation of atmospheric transmissivity that only uses ground elevation with respect to mean sea level instead of T_a and actual vapour pressure, as in the Brutsaert (1975) model. In the Stefan-Boltzmann equation [$\varepsilon_a\ \sigma\ (T_a)^4$] used in the computation of $R_{lw}\downarrow$, if T_s is used instead of T_a ($T_s > T_a$ in our case) then a higher temperature will be raised to the power of 4, thus augmenting the resulting $R_{lw}\downarrow$ beyond the value that would have been estimated had T_a been used. The result is that adding $R_{lw}\downarrow$ to the shortwave net radiation [$(1-\alpha)\ R_s$] would yield a higher sum had the proper temperature been used. For example, R_n estimate differences, for the SW lysimeters, were 81.6, 78.3, 73.2 and 49.2 W m^{-2} for $R_n(T_B)$, R_n(ME), R_n(MO), and R_n(MO2), respectively. This field was planted to dryland sorghum and had low biomass (LAI of 0.4–0.5 m^2 m^{-2}) and consequently displayed higher surface temperature than the irrigated NE, SE, and grass lysimeter fields where errors were much lower. The surface temperatures for the SW field were estimated to be 34.7°C using METRIC and 37.9°C using MODTRAN calibrations. Thus, METRIC-based T_s was 3.2°C lower than that estimated using MODTRAN, which resulted in underestimating $R_{lw}\uparrow$, i.e. [$\varepsilon_o\ \sigma\ (T_s)^4$]. Therefore, the $R_{lw}\uparrow$ term in the net radiation budget was smaller and this resulted in larger R_n than the measured value.

Table 2. Net radiation estimation errors for different T_s calibration methods[a]. Based on comparison to net radiometer data from five lysimeters.

Statistic	$R_n(T_B)$	R_n(ME)	R_n(MO)	R_n(MO2)
MBE (W m^{-2})	59.6	56.8	53.1	25.3
RMSE (W m^{-2})	17.7	17.2	15.5	19.4
MBE (%)	10.3	9.8	9.1	4.4
RMSE (%)	3.2	3.1	2.8	3.4

[a] $R_n(T_B)$ is T_B-based net radiation; R_n(ME) is T_s(ME)-based net radiation; R_n(MO) is T_s(MO)-based net radiation; R_n(MO2) is T_s(MO2)-based net radiation.

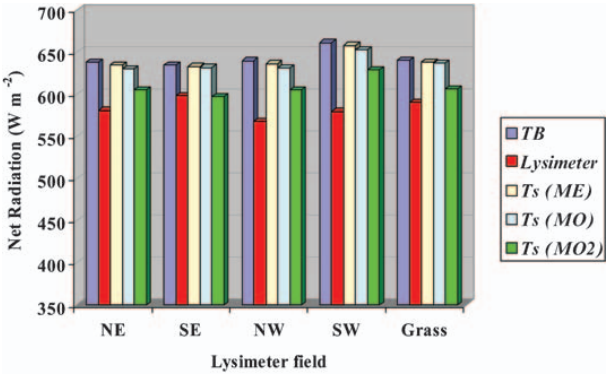

COLOUR FIGURE

Figure 3. Net radiation estimated using four different surface temperature methods.

Figure 3 displays R_n values estimated using the four different methods. In this figure, method R_n(MO2), i.e. R_n estimated with the T_s(MO2) method, compared better to measured values. The maximum overestimation by the T_s(MO2) method was 49.2 W m^{-2} in the SW field planted to dryland grain sorghum, while the minimum overestimation was 15.9 W m^{-2} for the irrigated grass lysimeter field. Results for R_n(MO2) matched well with measured R_n at the irrigated SE forage sorghum field. The SE lysimeter's field showed large biomass on DOY 204. It should be noted that radiometric surface temperature corrections for atmospheric interference are exponential, i.e. they increase exponentially as surface temperature increases; also less correction is applied to lower surface temperatures and vice versa (Chávez *et al.* 2005). The results shown in figure 3 and table 2 suggest that further atmospheric correction is needed on the at-sensor surface brightness temperature image. Better corrections may be attained with MODTRAN if atmospheric gas concentrations are regularly updated in the software to better characterize actual atmospheric conditions.

METRIC-estimated α matched measured values very closely (table 3). To validate LAI, measured values at the SE field (forage sorghum) were used. On average measured LAI was 3.9 m^2 m^{-2} for this field, hence an indication that the local model (Gowda *et al.* 2007b) may have the ability to accurately estimate LAI for high biomass fields, although both LAI(ME) and LAI(THP) underestimated the LAI by about 54% for the NE corn field (table 3). This large LAI underestimation error on sparse, low biomass vegetation may have contributed to net radiation estimation

Table 3. Comparison of albedo and LAI estimates.

Lysimeter	Measured albedo (α)	METRIC albedo (α)	LAI(measured) (m^2 m^{-2})	LAI(ME)[a] (m^2 m^{-2})	LAI(THP)[b] (m^2 m^{-2})
NE	0.17	0.17	0.8	0.35	0.38
SE	0.17	0.18	3.9	6.00	4.20
NW	0.16	0.16	N/A	0.30	0.33
SW	0.16	0.14	N/A	0.40	0.52
Grass	—	0.18	N/A	2.30	2.98

[a]LAI(ME) is leaf area index estimated using the METRIC equation (13).
[b]LAI(THP) is leaf area index estimated using the Texas High Plains LAI equation (12).

errors on the NE, NW and SW fields, and to errors in the estimation of G and H fluxes.

3.3 *Estimation of the* d*T function*

Four distinct functions relating T_s to dT were found with different T_s corrections, as highlighted in §2.6.

For T_s values corresponding to surfaces ranging from open water bodies (coldest) to bare/fallow soils (hottest), it is evident that smaller dT values, i.e. (T_{aero}–T_a), were obtained as corrections to T_B were made, i.e. surface emissivity correction followed by atmospheric corrections (figure 4). A smaller regression slope was obtained using T_s(MO) since corrections made were greater for higher surface temperature values. In the case of T_s(MO2), the local LAI and Z_{om} models contributed to decreasing dT values even further, although the dT decrement was greater for smaller T_s values than for larger values, when compared with dT values from the T_s(MO) line.

A sample of different inputs/outputs from estimating dT and H, for the T_s(ME) method, is shown in Appendix A (tables A1 and A2). For the cold pixel H was $-65.7\ \mathrm{W\,m^{-2}}$, i.e. indication that advection occurred in the region (table A2). Thus, 11.2% more energy (on top of the available energy (R_n–G)) was added from local/regional advected heat; thus resulting in an enhancement of ET in the same magnitude.

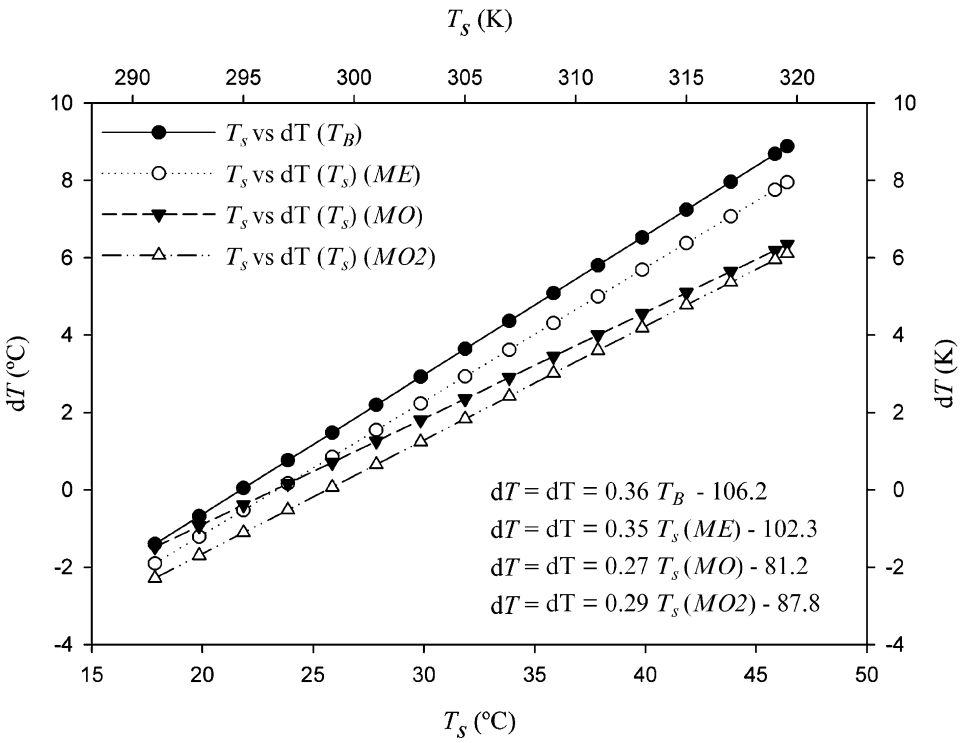

Figure 4. Relationship between dT and T_s for different radiometric surface temperature calibrations.

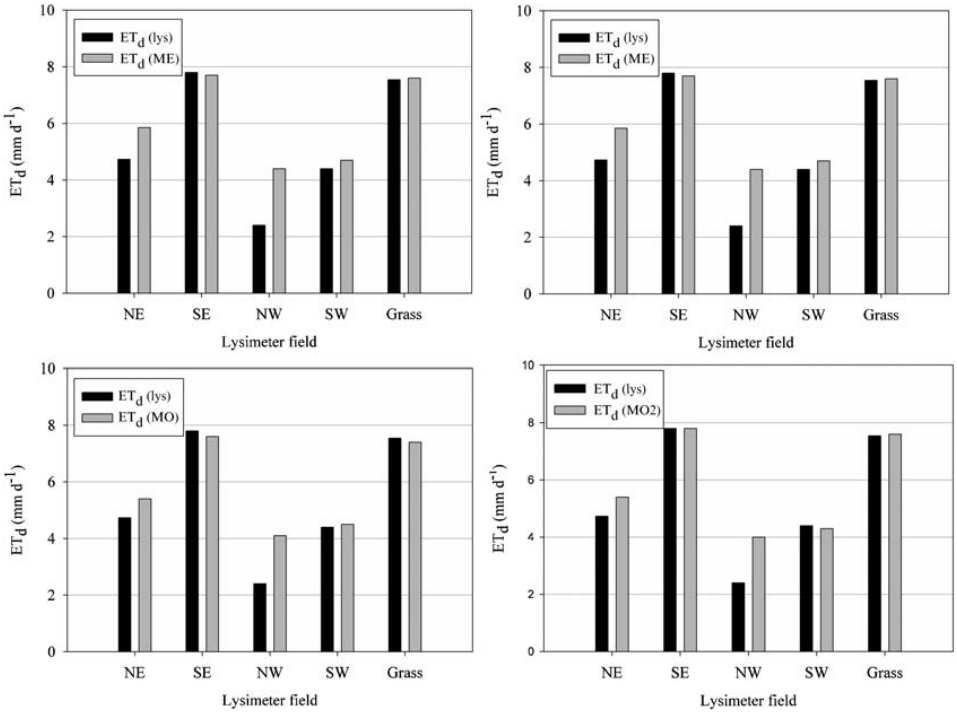

Figure 5. Remote sensing-based daily ET estimation using four different surface temperature calibration methods.

3.4 *Daily ET estimation*

Comparisons of estimated ET_d values with lysimeter data are shown in figure 5, where ET_d(lys) represents lysimeter data. In this figure, it appears that ET_d(MO2) (daily ET estimated using T_s(MO2)) better matched the measured values. This method resulted in somewhat large errors, i.e. $0.4 \pm 0.7\,\mathrm{mm\,d^{-1}}$ or $15.9 \pm 29.1\%$, but similar to those from T_s(MO) and smaller than those from T_s(ME) and T_B-based methods. T_s(MO) resulted in similar errors of $0.4 \pm 0.8\,\mathrm{mm\,d^{-1}}$, while prediction errors with methods T_s(ME) and T_B were on average $7 \pm 5\%$ greater than those of T_s(MO2) and T_s(MO) (table 4). ET prediction bias was larger for the NW lysimeter irrespective of the method used for deriving surface temperature. This may be partly due to errors in the estimation of aerodynamic resistance and surface roughness length for the clumped grain sorghum in the NW lysimeter field.

When ET_d results were analysed by excluding data from the NW lysimeters (table 5), ET prediction errors decreased to $0.2 \pm 0.35\,\mathrm{mm\,d^{-1}}$ or $3.2 \pm 7.4\%$ for the

Table 4. Comparison of ET_d for different T_s calibration methods using ET data from five lysimeters.

Statistic	$ET_d(T_B)$	$ET_d(T_s)$(ME)	$ET_d(T_s)$(MO)	$ET_d(T_s)$(MO2)
MBE (mm d^{-1})	0.72	0.68	0.43	0.45
RMSE (mm d^{-1})	0.94	0.88	0.79	0.71
MBE (%)	24.1	22.7	16.6	15.9
RMSE (%)	37.1	35.3	33.1	29.1

Table 5. Comparison of ET_d for different T_s calibration methods using ET data from four lysimeters (excluding lysimeter field NW data).

Statistic	$ET_d(T_B)$	$ET_d(T_s)$(ME)	$ET_d(T_s)$(MO)	$ET_d(T_s)$(MO2)
MBE (mm d^{-1})	0.37	0.35	0.11	0.20
RMSE (mm d^{-1})	0.62	0.54	0.40	0.35
MBE (%)	8.28	7.50	3.00	3.17
RMSE (%)	12.66	11.32	7.74	7.44

ET_d(MO2) method and to 0.1 ± 0.40 mm d^{-1} (3.0 ± 7.7%) for the ET_d(MO) method. ET_d(ME) and $ET_d(T_B)$ methods on average showed 5 ± 5% larger errors than those of ET_d(MO2) and ET_d(MO).

These results are evidence that the dT mechanism works well when T_B is properly corrected for atmospheric effects and surface emissivity; and when the aerodynamic resistance, r_{ah}, is spatially estimated using locally developed LAI and Z_{om} models. This contradicts the findings by Allen *et al.* (2005b) and Tasumi *et al.* (2005) that the dT mechanism cancels errors introduced by not calibrating T_s for atmospheric effects with a radiative transfer model (and radiosonde data), and propagation of those errors in the estimation of R_n and G.

Furthermore, when ET_d was estimated using the T_s(MO2) method, the MBE was 0.0% for the irrigated SE-sorghum field, below 1.0% for the irrigated grass field, −2.3% for the SW field, while it was 14.2% for the NE field, which had lower biomass (LAI~0.8 m^2 m^{-2}, late planted silage corn). This is in agreement with Allen *et al.* (2005b) that METRIC works better for larger ET rates than for midrange values.

Finally, the spatial variability of daily ET is displayed in figure 6, where the difference between irrigated and dryland regimes for sorghum and corn crops is evident within the lysimeter fields. The ET_d values were, 7.8 mm d^{-1} for the irrigated silage sorghum field (SE lysimeter area), 5.4 mm d^{-1} for irrigated corn (NE lysimeter area), 4.3 mm d^{-1} for grain sorghum (SW lysimeter), 4.0 mm d^{-1} for clumped grain

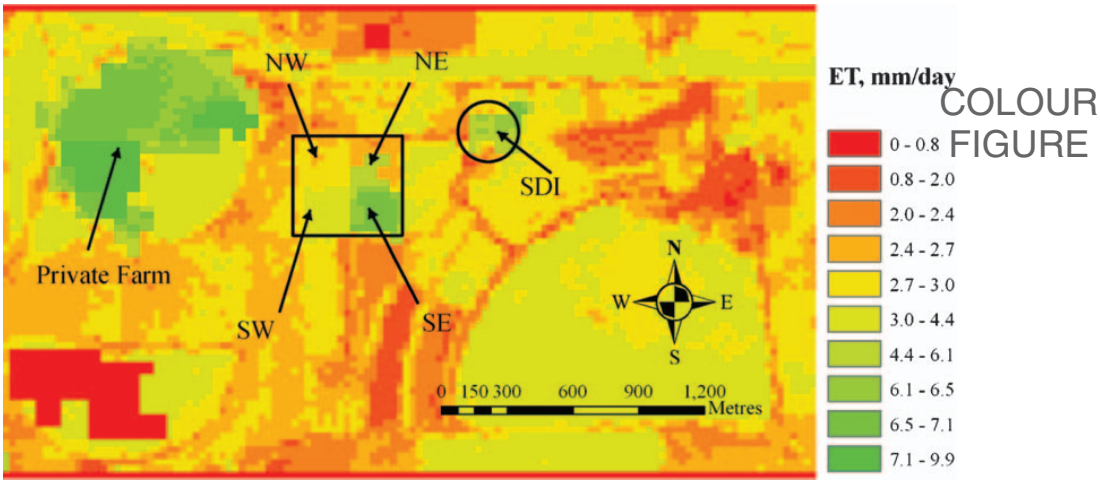

Figure 6. Spatially distributed daily ET on 23 July 2006 covering part of the USDA-ARS-CPRL and an adjoining private farm (centre pivots) to the west. The lysimeter fields are marked within the rectangle.

sorghum (NW lysimeters), and 7.6 mm d^{-1} of ET_d for the grass lysimeter field. Greater ET_d rates, up to 9.9 mm d^{-1}, can be observed on the centre pivot-irrigated silage sorghum belonging to the private farm located to the west of the lysimeter fields. In addition, ET_d was 7.2–7.8 mm d^{-1} for the sub-surface drip irrigation (SDI) irrigated corn plots to the east of the lysimeter fields.

4. Conclusions

The METRIC algorithm was applied using a Landsat 5 TM image acquired on 23 July 2006 at 11:20 CST (17:20 GMT) hours. MODTRAN-calibrated T_s values compared better with observed data than did values obtained using corrections made with default METRIC algorithms. Errors in obtaining T_s with MODTRAN were -1.9 and 0.4% for lysimeter fields NE and SE, respectively, while with METRIC submodel, errors were -11.1 and -1.9%, respectively. Larger biases were found for higher surface temperature on the low biomass NE corn lysimeter field, perhaps due to uncertainties in mix soil/vegetation thermal emissivity values and errors in the estimation of vegetation indices due to soil background effects.

ET_d estimates closely matched measured values at four lysimeter locations (MBE $\pm$ RMSE values were 0.4 ± 0.35 mm d^{-1} or 3.2 ± 7.4%), showing discrepancies for the clumped grain sorghum field (NW lysimeter). Considering the ET data of all five lysimeters, the smallest ET_d estimation error was 0.4 ± 0.7 mm d^{-1} (15.9 ± 29.1%) for the T_s(MO2) method, where at-sensor brightness surface temperatures were corrected for atmospheric effects and surface thermal emissivity using the MODTRAN4 model, and when region-specific LAI and surface roughness length models were applied. The largest bias in ET_d estimation occurred when no corrections were made to the satellite brightness surface temperature image. Thus, the results obtained in this study indicate that proper satellite thermal band calibration is needed, in conjunction with locally calibrated plant LAI and aerodynamic roughness models, in order to obtain more accurate spatial crop ET estimates.

Overall, the use of METRIC for the advective conditions of the THP is promising.

References

ALLEN, R.G., TASUMI, M., MORSE, A. and TREZZA, R., 2005a, Satellite-based energy balance and evapotranspiration model in Western US water rights regulation and planning. *Irrigation and Drainage Systems*, **19**, pp. 251–268.

ALLEN, R.G., TASUMI, M. and TREZZA, R., 2005b, *METRIC: Mapping evapotranspiration at high resolution—Applications manual for Landsat satellite imagery*. University of Idaho, Kimberly, Idaho, USA.

ALLEN, R.G., TASUMI, M. and TREZZA, R., 2007, Satellite-based energy balance for mapping evapotranspiration with internalized calibration (METRIC)—Model. *ASCE Journal of Irrigation and Drainage Engineering*, **133**, pp. 380–394.

ASCE-EWRI, 2005, The ASCE standardized reference evapotranspiration equation. Report by the American Society of Civil Engineers (ASCE) Task Committee on Standardization of Reference Evapotranspiration. R.G. Allen, I.A. Walter, R.L. Elliot, T.A. Howell, D. Henfisu, M.E. Jensen, and R.L. Snyder (Eds), (Reston, VA: ASCE).

AXTELL, S., 2006, *Ogallala Initiative*. United States Department of Agriculture—Agricultural Research Service (USDA-ARS). Available online at: http://ogallala.tamu.edu (accessed 20 November 2006).

BASTIAANSSEN, W.G.M., 1995, Regionalization of surface flux densities and moisture indicators in composite terrain: A remote sensing approach under clear skies in Mediterranean climates. PhD dissertation, Wageningen Agricultural University, Wageningen, The Netherlands. CIP Data Koninklijke Blibliotheek, Den Haag.

BASTIAANSSEN, W.G.M., 2000, SEBAL-based sensible and latent heat fluxes in the irrigated Gediz Basin, Turkey. *Journal of Hydrology*, **229**, pp. 87–100.

BASTIAANSSEN, W.G.M., MENENTI, M., FEDDES, R.A. and HOLTSLANG, A.A., 1998, A remote sensing surface energy balance algorithm for land (SEBAL): 1. Formulation. *Journal of Hydrology*, **212–213**, pp. 198–212.

BERK, A., BERNSTEIN, L.S. and ROBERTSON, D.C., 1989, MODTRAN: a moderate resolution model for LOWTRAN 7. Report GL-TR-89-0122. Geophysics Laboratory, Bedford, Maryland, USA.

BERK, A., ANDERSON, G.P., ACHARYA, P.K., HOKE, M.L., CHETWYND, J.H., BERNSTEIN, L.S., SHETTLE, E.P., MATTHEW, M.W. and ADLER-GOLDEN, S.M., 2003, MODTRAN4 Version 3 Revision 1 User's Manual. Air Force Research Laboratory, Space Vehicles Directorate, Air Force Material Command, Hanscom AFB, MA 01731-3010, Hanscom.

BORAK, J.S., JASINSKI, M.F. and CRAGO, R.D., 2005, Time series vegetation aerodynamic roughness fields estimated from MODIS observations. *Agricultural and Forest Meteorology*, **135**, pp. 252–268.

BRUTSAERT, W., 1975, On a derivable formula for long-wave radiation from clear skies. *Water Resources Research*, **11**, pp. 742–744.

BRUTSAERT, W.H., 1982, *Evaporation into the Atmosphere* (Boston, MA: D. Reidel).

CHANDER, G. and MARKHAM, B., 2003, Revised Landsat-5 TM radiometric calibration procedures and postcalibration dynamic ranges. *IEEE Transactions on Geoscience and Remote Sensing*, **41**, pp. 2674–2677.

CHÁVEZ, J.L., 2005, Validating surface energy balance fluxes derived from airborne remote sensing. PhD dissertation, Utah State University, Logan, Utah, USA.

CHÁVEZ, J.L., NEALE, C.M.U., HIPPS, L.E., PRUEGER, J.H. and KUSTAS, W.P., 2005, Comparing aircraft-based remotely sensed energy balance fluxes with eddy covariance tower data using heat flux source area functions. *Journal of Hydrometeorology*, **6**, pp. 923–940.

DENNEHY, K.F., 2000, High Plains regional ground-water study: US Geological Survey Fact Sheet 091-00.

FOKEN, T., 2006, 50 Years of the Monin-Obukhov similarity theory. *Boundary-Layer Meteorology*, **119**, pp. 431–447.

GOWDA, P.H., CHAVEZ, J.L., COLAIZZI, P.D., EVETT, S.R., HOWELL, T.A. and TOLK, J.A., 2007a, ET mapping for agricultural water management: Present status and challenges. *Irrigation Science*, **26**, pp. 223–237.

GOWDA, P.H., CHAVEZ, J.L., COLAIZZI, P.D., HOWELL, T.A., SCHWARTZ, R. and MAREK, T.H., 2007b, Relationship between LAI and Landsat TM spectral vegetation indices in the Texas Panhandle. Paper number 072013. In *Proceedings of the 2007 ASABE Annual International Meeting*, 17–20 June 2007, Minneapolis, Minnesota, USA (St Joseph, Michigon: ASABE).

GUEYMARD, C., 1995, SMARTS2. A simple model of the atmospheric radiative transfer of sunshine: algorithms and performance assessment. Professional Paper FSEC-PF-270-95. Florida Solar Energy Center, University of Central Florida.

HOWELL, T.A., SCHNEIDER, A.D., DUSEK, D.A., MAREK, T.H. and STEINER, J.L., 1995, Calibration and scale performance of Bushland weighing lysimeters. *Transactions of the ASAE*, **38**, pp. 1019–1024.

MCGUIRE, V.L., 2004, Water-level changes in the high plains aquifer, predevelopment to 2003 and 2002 to 2003. US Geological Survey Fact Sheet FS-2004-3097. Available online at: http://pubs.usgs.gov/fs/2004/3097 (accessed 8 December 2006).

NORMAN, J.M., KUSTAS, W.P. and HUMES, K.S., 1995, A two-source approach for estimating soil and vegetation energy fluxes in observations of directional radiometric surface temperature. *Agricultural and Forest Meteorology*, **77**, pp. 263–293.

SULEIMAN, A. and CRAGO, R., 2002, Analytical land atmosphere radiometer model (ALARM) applied to a dense canopy. *Agricultural and Forest Meteorology*, **112**, pp. 151–159.

SULEIMAN, A. and CRAGO, R., 2004, Hourly and daytime evapotranspiration from grassland using radiometric surface temperatures. *Agronomy Journal*, **96**, pp. 384–390.

SUMMER, D.M. and JACOBS, J.M., 2005, Utility of Penman-Monteith, Priestley-Taylor, reference evapotranspiration, and pan evaporation methods to estimate pasture evapotranspiration. *Journal of Hydrology*, **308**, pp. 81–104.

TASUMI, M., TREZZA, R., ALLEN, R.G. and WRIGHT, J.L., 2005, Operational aspects of satellite-based energy balance models for irrigated crops in the semi-arid US. *Journal of Irrigation and Drainage Systems*, **19**, pp. 355–376.

TXHPET 2006, Texas High Plains Evapotranspiration Network. Available online at: http://txhighplainset.tamu.edu/index.jsp (accessed 4 September 2006).

TOLK, J.A., EVETT, S.R. and HOWELL, T.A., 2006, Advection influences on evapotranspiration of alfalfa in a semiarid climate. *Agronomy Journal*, **98**, pp. 1646–1654.

TREZZA, R., 2002, Evapotranspiration using a satellite-based surface energy balance with standardized ground control. PhD dissertation, Utah State University, Logan, Utah, USA.

YANG, R. and FRIEDL, M.A., 2002, Determination of roughness lengths for heat and momentum over Boreal forests. *Boundary-Layer Meteorology*, **107**, pp. 581–603.

Appendix A: d*T* estimation input/output sample

Table A1 shows the input data used in the initial estimation of dT and H, for the T_s(METRIC) method, for both hot and cold pixels under neutral atmospheric conditions. Initial H and dT values were subsequently adjusted for the unstable atmospheric conditions encountered for DOY 204 using the Monin-Obukhov length scale iterative method. After five iterations, changes in r_{ah} for the hot pixel satisfied the convergence criteria of 5% difference in r_{ah} for each iteration cycle. In addition, table A2 reports the resulting final values for r_{ah}, horizontal friction velocity (u_*), L_{MO}, dT, LE, and H for both cold and hot pixels.

Table A1. METRIC input table for H determination.

Variable	Units	Cold pixel	Hot pixel
Coordinates	X (UTM), m	763483.4	764730.6
Coordinates	Y (UTM), m	3897854.6	3895811.8
Elevation	m	1170	1170
Albedo	dimensionless	0.21	0.24
LAI	$m^2\,m^{-2}$	5.3	0.06
ET_rF	dimensionless	1.05	0
T_s	K	291.6	315.1
R_n	$W\,m^{-2}$	615.9	554.2
G	$W\,m^{-2}$	29.3	130.2
Z_{om}	m	0.11	0.005
u (200 m)	$m\,s^{-1}$	5.84	5.84

Table A2. METRIC atmospheric stability adjusted H.

Variable	Unit	Cold pixel	Hot pixel
r_{ah}	$s\,m^{-1}$	26.1	14.9
u_*	$m\,s^{-1}$	0.31	0.33
L_{MO}	m	33.4	−6.6
dT	K	−1.63	6.49
LE	$W\,m^{-2}$	652.3	0.0
H	$W\,m^{-2}$	−65.7	424.0